

Dual Species Effusive Source and Zeeman Slower for Cold Atom Experiments

William Bowden,* Will Gunton, Mariusz Semczuk, Kahan Dare, and Kirk W. Madison
The Department of Physics and Astronomy, University of British Columbia, Vancouver, Canada

(Dated: December 8, 2024)

We present a dual-species effusive source and Zeeman slower capable of producing slow atomic beams of two elements with a large mass difference, and we realize this design to slow and load ${}^6\text{Li}$ and ${}^{85}\text{Rb}$ into a magneto-optical trap. Key design choices, such as separating the effusive sources and allowing for the computer control of the magnetic field profile, ensure that the apparatus can be easily modified to facilitate the cooling of alternative atomic species making it applicable for a variety of cold atom experiments. By utilizing the quadrupole magnetic field of the magneto-optic trap as a secondary slowing field, we are able to shorten our Zeeman slower making for a more compact and robust system without compromising performance. Secondary slowing by the MOT trapping field is optimized by tuning the exit speed of atoms from the Zeeman slower through the use of a disengagement coil. We outline the construction and analyze the emission properties of our effusive sources. Finally, we verify the performance of the source and slower by measuring the loading rate and steady state atom number of a magneto-optical trap of both species. We achieve a maximum loading rate of 3.5×10^8 atoms/s for Rb and 2×10^7 atoms/s for Li, consistent with the expected performance of the slower at the operational temperatures of the effusive sources.

The ability to trap and cool multiple species simultaneously has garnered much interest within the cold atom community because the complex interactions within these systems give rise to a diverse range of physical phenomena. Quantum degenerate Fermi-Fermi [1, 2], Fermi-Bose [3–6], and Bose-Bose [7–9] gases allow for the study of novel states of matter which cannot be investigated in single species experiments. In particular, mixtures with large mass ratios, like those species presented here, are of interest for many body physics in the study of superfluidity[10], spin impurities, and Effimov physics [11]. Unfortunately, large mass differences also results in practical challenges when trying to slow multiple species.

Abundant samples of cold atoms are also a prerequisite for the formation of ultracold hetero-nuclear molecules [12–14] whose long range dipole-dipole interactions lead to exotic phases of matter and possible quantum information applications [15–17]. LiRb is an excellent candidate for such studies as it is predicted to have the second largest electric inherent dipole moment of the alkali dimers and when in the triplet state has the added advantage of a magnetic dipole moment [18]. Furthermore, for certain experiments, there are practical advantages to having the ability to trap multiple species. For example, one species with poor collisional properties (which limit the efficacy of evaporative cooling) can be cooled sympathetically via interactions with the other species [19–22]. In other cases, one species can serve as an atomic detector to measure properties of the system, as has been demonstrated for thermodynamic measurements [23, 24].

Given the increased experimental complexity which comes with cooling and trapping multiple species simultaneously, it is desirable to design systems which are simple, quick to assemble, and robust. A necessary starting point for such experiments are cold atomic samples con-

finied within a magneto-optical trap (MOT). Here, we focus on the creation of such samples through the use of a dual species Zeeman slower which can effectively slow the hot samples produced by effusive sources. Although this apparatus was constructed for the cooling of ${}^6\text{Li}$ and ${}^{85}\text{Rb}$, the general design is easily adapted to different atomic species because the effusive sources are separate and can be easily switched, and the magnetic field profile is computer controlled and can be modified without any physical changes to the slower.

Section 1 of this paper describes the design and construction of the Zeeman slower and effusive sources while highlighting some important considerations when designing multi-species cold atom experiments. Section 2 validates the performance of the system by loading MOTs of both species and discusses the results and their implications for slowing other atomic species.

I. DESIGN AND CONSTRUCTION

A. Effusive Sources

Effusive sources are a common starting point for most laser cooling experiments and accurately predicting their emission properties is critical to ensuring proper performance. Reloading the source after its depletion is a non-trivial task as it can potentially compromise the vacuum and often requires baking all or part of the system to achieve the desired base pressure. For this reason, it is desirable to maximize the lifetime of the effusive source without reducing the center line intensity of the atomic beam. One common approach is to use a recirculating or candlestick source where thermal gradients wick back and recollect atoms which are emitted off-axis [25]. The downside of such sources is their complexity in design and operation. An alternative is the use of arrays of large aspect ratio microtubes. The microtubes collect the ma-

* william.bowden@physics.ox.ac.uk

majority of atoms exiting off-axis and emit some fraction back into the reservoir without compromising the center line intensity of the atomic beam. This increases the longevity of the source without reducing loading rates.

In the regime where the mean free path of atoms is much longer than the length of the tube, the rate at which atoms are emitted from the effusive source through an opening of area A containing an atomic vapor of density n with mean velocity \bar{v} is

$$N = \frac{nA\kappa\bar{v}}{4}, \quad (1)$$

where the parameter κ is the Clausing factor and is derived from the geometry of the exit channel [26, 27]. The design of such effusive sources for multi-species Zeeman slowers is complicated since they require collinear atomic beams. One approach is to connect multiple reservoirs to a common mixing chamber where the atoms exit via the same opening [28]. The steady state flux of the various species out of the effusive source is controlled by the rate they enter the mixing chamber. Care needs to be taken to prevent back flow between reservoirs and possible chemical reactions within the mixing chamber. Furthermore, the temperature of the mixing chamber must be kept warmer than the hottest reservoir to prevent condensation, which results in a higher mean velocity for atoms leaving the source than could otherwise be achieved with separate sources. This is especially problematic when the elements have vastly different vapor pressures at a given temperature, as it is the case when working with most alkali and alkali-earth mixtures. We elected to follow an alternative approach demonstrated by Wille et al. [29] of having separate sources with no mixing chamber to avoid such complications while still producing parallel and overlapping atomic beams by offsetting slightly their output ports. This ensures our design is easily adapted to accommodate different atomic species.

To simplify the design, the entire Li source and the majority of the Rb source was made from off-the-shelf vacuum components. The Li source was made from a 1.33" ConFlat nipple sealed on both sides with a ConFlat blank. A 4 mm \times 2 mm oval was milled into the blank which connects the source to the apparatus into which approximately 60 microtubes are press fitted. The tubes are 1 cm in length with an inner (outer) diameter of 200 (300) μm . Unlike other microtube designs which require a retaining plug or bar [30], we found that press fitting the tubes held them sufficiently secure and well aligned. All gaskets within the Li oven are made from annealed nickel because copper cannot maintain a UHV seal as it is quickly corroded by the hot Li. During initial testing, copper gaskets were used and failed within a few hours to days depending on the operational temperature. Prior to loading the source, the Li (which was stored in a petroleum ether) was cleaned inside an argon filled glove bag by rinsing it in acetone and then cleaving off the outer oxidized layers. Approximately 3 g of Li

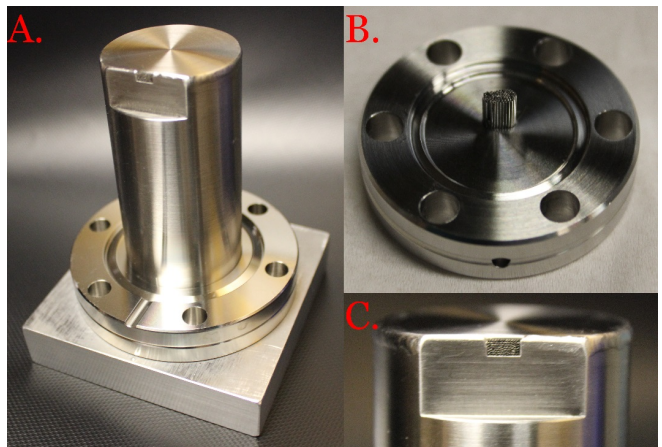


FIG. 1. Key components of the effusive sources: (A) Rb oven with microtube array, (B) Li oven cap with microtube array, (C) close up of Rb microtube array.

was loaded into the oven, which gives an estimate source lifetime of four years at a continual operational temperature of 450°C. Common to most microtube sources, the outlet is kept warmest to prevent clogging. However, the resulting temperature gradient leads to thermal wicking of the molten Li towards the hottest region (the outlet) as in the operation of a standard heat pipe. During testing, we observed molten Li being pulled through the microtube opening by capillary action which completely depleted the source. To prevent this, we lined the oven with a nichrome mesh to which Li preferentially adheres and helps to ensure it remains in the source. The mesh ensures that even with large temperature gradients, the liquid Li remains confined to the inside of the source and does not contact the microtubes.

The Rb source is slightly more complex in design as the sample, which has a very high vapour pressure at elevated temperatures, must remain sealed in a glass ampule which is broken in-situ after the bakeout process. The ampule's base and top are held by two modified CF-blanks connected by a flexible bellows which is used to crack the ampule [31]. In order for the Rb and Li atomic beams to be parallel and only slightly offset, the bellows is connected to a hollow stainless cylinder which extends into the vacuum system and ends directly below the Li exit channel. A 4 mm \times 2 mm opening is milled into a stainless steel cap, which is then TIG welded onto the top of the cylinder prior to being press fitted with microtubes. The key components of both sources are shown in Figure 1.

B. Dual Species Zeeman Slower

Zeeman slowers have been used extensively in ultra-cold atom experiments to produce beams of slow atoms as they are simple to construct, require relatively low power in the slowing lasers, and are robust against de-

variation in magnetic field or misalignment. Alternative approaches for loading MOTs include transferring atoms from a 2D MOT [32, 33], loading atoms directly from a background pressure produced by a dispenser [34], and capturing the unslowed atomic beam emitted by an oven [35]. The 2D MOT approach has been successfully implemented for loading multiple species [36, 37], but is significantly more complex and expensive than alternative designs (such as a Zeeman slower) primarily due the high power requirements for cooling. The dispenser approach is the simplest to implement, but only works for species with appreciable vapor pressure at room temperature such as Rb. For elements such as Li where the vapor pressure is exceedingly low at room temperature, an oven producing an atomic beam with direct line of sight to the MOT is required. Having dispensers or atomic ovens close to the trapping region can result in higher background pressures that limit the trap lifetime and thus the achievable atom number in the MOT [38, 39]. However, such an approach has proven successful in the production of degenerate gases of ${}^6\text{Li}$ [40].

By placing the atomic oven further away from the trapping region, differential pumping techniques can be used to reduce the contribution of the background pressure in the trapping region due to the hot atomic sources. To offset the reduction in the trappable atom flux resulting from moving the oven away from the MOT, a Zeeman slowing stage is used to slow fast moving atoms to a velocity which can be captured by the trap.

Zeeman slowers are classified as one of three types depending on the polarization of the slowing light and magnetic field which in turn determines the atomic transition that is used for slowing. The classifications are σ^+ (decreasing magnetic field), σ^- (increasing magnetic field), and spin-flip (magnetic field has zero crossing at some point in the slower) [41]. The magnetic field profile for the σ^+ slower, which is presented in this work, is given by

$$B(z) = \frac{\hbar k v_c}{\mu} \sqrt{1 - \frac{2z}{m v_c^2}} - \frac{\hbar \delta}{\mu} \quad (2)$$

where k is the wavevector of the slowing beam, v_c is the capture velocity of the slower (i.e. the largest velocity class it can slow), μ is the magnetic moment of the transition, a is the deceleration, and δ is the laser detuning. The upper limit on deceleration, a_{max} , imposed by the finite scattering rate constrains the maximum magnetic field gradient which can be used for slowing to

$$\left| \frac{dB(z)}{dz} \right| \ll \frac{\hbar k a_{max}}{\mu v(z)}, \quad (3)$$

commonly referred to as the adiabatic slowing condition [42]. In practice, the magnetic field is stretched spatially by a factor η which relates the deceleration experienced by the atoms to a_{max} via $a = \eta a_{max}$. If this gradient is exceeded, atoms will fall out of resonance with the

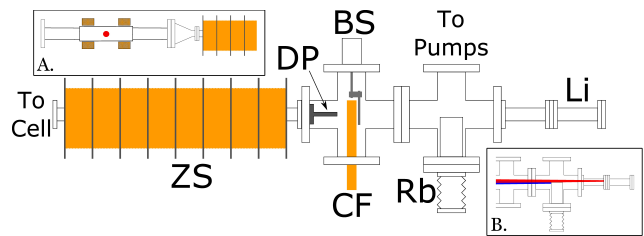


FIG. 2. Experimental apparatus showing the two effusive sources (Li, Rb), cold finger (CF), beam shutter (BS), differential pumping tube (DP), and Zeeman slower (ZS). The inset shows the trajectory of the two atomic beams for reference. Inset A shows the location of the MOT, as indicated by the red circle, within the science section connected to the end of the slower. Inset B shows co-propagating atomic beams from the effusive sources.

slowing beam and will stop decelerating. In this work, we actually use this phenomenon to disengage the atoms from the slower to ensure they are not stopped or turned around before reaching the MOT. The unintended stopping and reversing of the atomic trajectories in the Zeeman slower is a primary consideration when optimizing its performance.

The maximum gradient is typically different for various atomic species which limits the feasibility of simultaneous slowing. In general, the ratio

$$\frac{\eta_1}{\eta_2} = \frac{m_1 \mu_1 k_2 \Gamma_2}{m_2 \mu_2 k_1 \Gamma_1}, \quad (4)$$

must be close to unity for efficient simultaneous slowing. For Li and Rb this ratio is 0.04 (predominantly due to the large mass difference). This greatly reduces the effectiveness of simultaneous slowing by using a fixed current or permanent magnets [43] design. Simultaneous slowing of the Li and Rb has been demonstrated, but it requires the magnetic field to be tailored such that specific regions along the slower cool different species [44]. Alternatively, one could use multiple Zeeman slowers at the expense of reduced optical axis [45]. Instead, we chose to dynamically switch the magnetic field profile to load the MOT and optical dipole trap (ODT) sequentially. Although this results in slightly longer experimental cycle time, we can achieve much larger samples as we can independently tune the MOT and Zeeman slower to the optimal loading parameters for both species. This sequential loading technique has been shown to be an effective approach to trapping Li and Rb in an ODT [46].

We elected to use a σ^+ design as the decreasing magnetic field has two main advantages. First, as a result of the atoms moving fastest in the large magnetic field region where the Zeeman effect almost cancels the Doppler shift, the required detuning of slowing beam is small and can be easily derived from our MOT lasers using an acousto-optic modulator. Second, the decreasing field can be mated with the increasing magnetic field from the MOT extending radially outwards such that atoms are

further decelerated by the Zeeman slowing beam when entering the MOT trapping region. Using the MOT field to provide slowing has been used in our previous experimental apparatus [40] and in similar dual species slowers [47].

Critical to the success of this design, we use a coil at the end of the slower to produce a magnetic field with opposite polarity to disengage atoms from the slower by violating the adiabatic slowing condition. By varying the current, we can control the velocity at the point of disengagement to ensure the atoms are resonant with slowing laser when reaching the MOT magnetic field. Using the MOT field for slowing has the added benefit that the final stage of slowing is done close to the trapping region which helps to mitigate the blooming of the atomic beam. Blooming occurs because the slower reduces the velocity component parallel to the axis of the slower while heating the radial velocity distribution due to spontaneous re-emission of the absorbed light. This leads to an increasing divergence of the atomic beam as the atoms decelerate. The result of this is that the divergence angle of the beam upon leaving the slower (proportional to ratio of initial velocity to the final velocity) is continuously increased with more slowing which counteracts the benefit of lengthening the slower in order to capture and slow atoms with even higher initial velocities.

To produce the Zeeman slower field, we elected to use eight solenoids with computer controlled currents allowing for automated optimization of the magnetic field. Motivated by the fact that elongating the slower to increase the capture velocity leads both to increasing power dissipation and to diminishing returns due to beam divergence, we elected to build a relatively short slower measuring 24 cm which is easily air cooled using the metal fins which separate the coils. The slower is typically operated with less than a fifty percent duty cycle, but we find that the fins provide sufficient heat transfer to the air such that the slower can be operated continuously at the largest required currents with the hottest coil only reaching a temperature of 60 °C.

One drawback of the σ^+ design compared to a σ^- and spin-flip slower, is that the slowing beam is much less detuned resulting in a larger radiation pressure exerted on the MOT. To reduce the radiation pressure, we focus the slowing beam at the entrance of the slower such that the beam is large at the MOT and the divergence more closely matches that of the atomic beam. This focussing has the added benefit that the beam curvature helps to provide some radial confinement.

Prior to constructing the slower, we simulated the atom trajectories as they decelerated within the slowing and trapping fields. The virtual slower adopts a two level model for the atom and solves the equation of motion subject to a positionally dependent radiation pressure. The result of the simulation is a bunching of atoms in phase space and can be used to estimate the proper current for the disengagement coil and slowing beam parameters. If the atoms leave the slower going too slowly

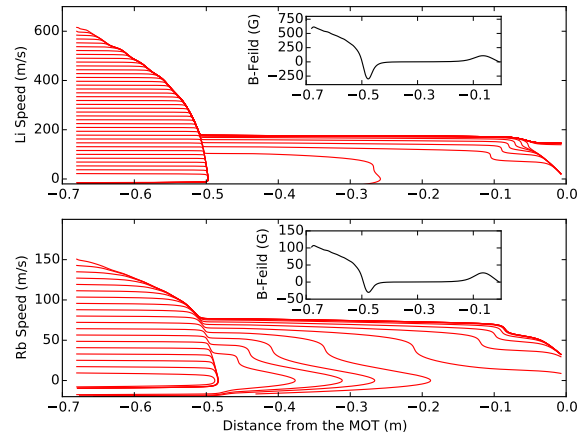


FIG. 3. Phase space trajectories for both species in the Zeeman slower and quadruple field of the MOT coils. The magnetic field was chosen to illustrate how improper choice of the disengagement coil current can cause atoms to either pass directly through without further slowing (top panel) because they leave the slower moving too quickly, or turn around before reaching the trap (bottom panel) because the atoms leave the slower moving too slowly. Inset figures show the magnetic field produced by the MOT coils and Zeeman slower

they risk the possibility of being turned around, while if they are traveling too fast they will not be captured by the MOT. The first effect is more likely for Rb as its exit velocity is lower than that of Li. These effects are illustrated in the phase space plots shown in Figure 3.

C. Vacuum System and Laser System

The Zeeman slower separates the science section of the experimental apparatus from the effusive source section. By decreasing the length of the slower, the isolation between the section is reduced requiring the addition of a differential pumping tube with an estimated hydrogen conductance of 1 L/s immediately before the slower. Both the source and science side are pumped by an Agilent VacIon Plus 20 Starcell ion pump and SAES CapaciTorr D 400-2 non-evaporatable getter.

The Li effusive source is loaded with Li and baked separately at 500 °C for 6 hours in order to remove any remaining mineral oil or contaminants from the loading process before being back filled with argon and attached to the main apparatus. The entire apparatus is then baked for one week at 200 °C.

Long term exposure of the ion pumps to a significant background pressure of Rb generates filaments that, through field emission, produce large leakage currents. This emission and heating limit the pumping performance by vaporizing the Rb and other materials originally stored in the pump. It has been suggested that the

lifetime of an ion pump exposed to a high vapor pressure of Rb can be prolonged by heating it continuously above its melting temperature [48]; however, we choose here to protect the pump by introducing a cold finger just after the Rb oven. Therefore, a copper feed through is placed inside the source section which is cooled externally using a TEC in order to condense Rb [49].

II. RESULTS AND DISCUSSION

A. The Effusive Source

Prior to assembling the entire apparatus, we measured the angular and velocity distribution of the emitted flux from the Li effusive source. To characterize the source, the emission was probed using a transverse laser which was scanned over the atomic D2 transition for the two ground hyperfine states. The flange containing the microtubes was heated to 450°C using metal band heaters while the opposite end was kept at approximately 15°C cooler. We developed a model [50] for the expected fluorescence signal based on the predicted angular and velocity distribution of the atoms leaving the effusive source. The expected angular distribution of a transparent channel of a given aspect ratio has been discussed in length in literature [27, 51, 52] and the velocity distribution, $F_{\text{MB}}^{\text{Beam}}(v)$, within the atomic beam emitted from a reservoir at a temperature T is [53]

$$F_{\text{MB}}^{\text{Beam}}(v) = \frac{m^2 v^3}{2k^2 T^2} \exp \left[- \left(\frac{2kTv}{m} \right)^2 \right]. \quad (5)$$

Based on the experimental data, the model estimates an average beam divergence of approximately 3° which corresponds to a microtube aspect ratio of approximately 20; half the expected value of 40 given the microtube diameter (250 μm) and length (1 cm). A possible explanation could be a slight misalignment between microtubes or emission from gaps between tubes where they are not well packed. The total flux of atoms at this operational temperature was measured to be 9×10^{15} atoms/s while the predicted value using Equation 1 is 4×10^{15} atoms/s which is in reasonable agreement as it neglects any emission from the gaps between tubes or uncertainty in source temperature. The Rb source was not tested prior to installation into apparatus as it required breaking the ampule.

Characterization of the effusive source with respect to atom loading rate, MOT lifetime, steady state atom number, and the lifetime of Li atoms loaded into an ODT at various operation temperatures was performed with optimized settings for the Zeeman slower. We note that the lifetime of atoms in the ODT (given by the inverse single-particle loss rate) is a better and more relevant proxy for the quality of the vacuum than the MOT lifetime as there are additional loss mechanisms present in the MOT

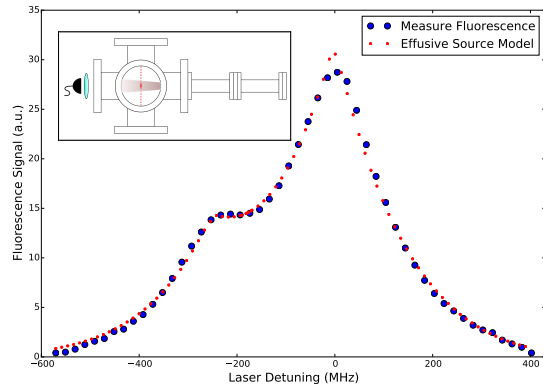


FIG. 4. Oven fluorescence produced by the probe beam along with our numerical model based on the expected angular and velocity distribution for the effusive source. The inset shows the experimental setup with the atomic beam going from right to left while probed by a transverse beam. In practice, the photodiode viewport is coated by Li during operation and it is best to place the detector along the other available axis orthogonal to the probe and atomic beams.

other than just collisions with background gases. These additional losses include light assisted collisions such as radiative escape and fine structure changing collisions, and they become more pronounced for larger MOT atom numbers where the atomic density is higher.

The Li oven temperature was increased while the Rb source was kept at room temperature. As the temperature increased, the loading rate and steady state atom number in the MOT increased while the ODT lifetime decreased steadily. At the lowest operating temperature (620 K), the Li MOT lifetime is more than a factor of 2 longer than the ODT lifetime. This is expected given the MOT trap depth is more than three orders of magnitude larger than the ODT [54]. However, as the source temperature is increased, the MOT number and density grows, and the light assisted collisional losses in the MOT become the dominant loss mechanism. The MOT lifetime is observed to then drop below the ODT trap lifetime. Once the steady-state number is large enough, the MOT grows in size with a constant density and the contribution to the single-particle loss rate (i.e. lifetime) from light assisted losses becomes constant. As the oven temperature is further increased, the ODT lifetime is reduced due to increased collisions with background gases emitted by the oven. Because the ODT depth is less than the MOT, the lifetime reduction is larger for the ODT than for the MOT [55].

To characterize the Rb slower, the Rb oven temperature was increased while the Li source was kept at a constant 630 K. The loading rate and steady state atom number increase monotonically while the ODT lifetime decreases. For the Rb MOT, the light assisted collisional losses are already dominant at the very lowest atom numbers (achieved at the lowest source temperature) and thus

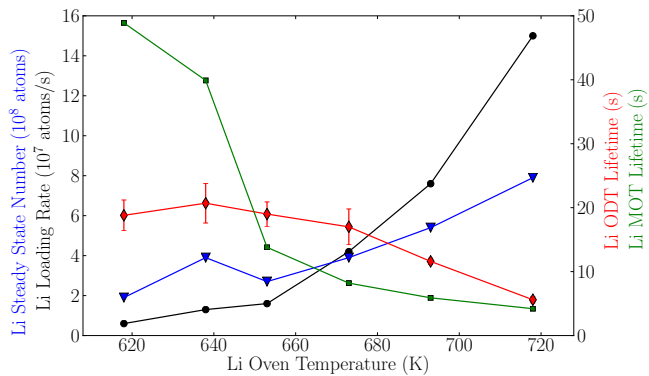


FIG. 5. The effect of Li source temperature of Li loading rate (black dots), steady state atom number (blue triangles), MOT lifetime (red diamonds), and ODT lifetime (green squares). Due to density dependent loss mechanism within the MOT, the lifetime of ODT is a better estimate of the background pressure inside the science section of the apparatus. Here the the Rb source is kept fixed at 290 K.

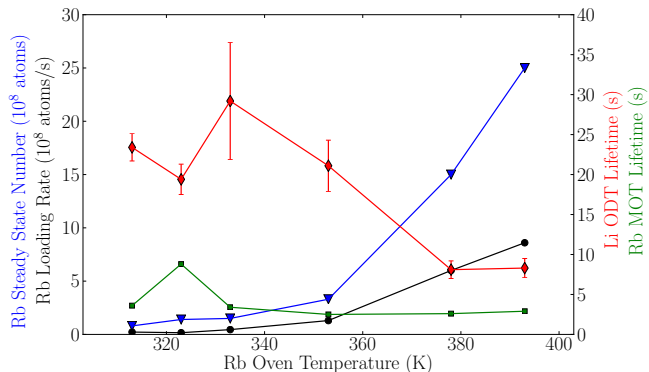


FIG. 6. The effect of Rb source temperature of Rb loading rate (black dots), steady state atom number (blue triangles), MOT lifetime (red diamonds), and lifetime for Li confined in a ODT (green squares). For rubidium, light assisted collisional losses are dominant for even the lowest density traps resulting in lifetimes shorter than those observed for the Li ODT. Here the Li source was held fixed at its standard operational temperature of 630 K.

the lifetime of a Rb atom in the MOT is always less than that of a Li atom in the ODT. Note that for these measurements, the Rb MOT was not present. Therefore, the Li lifetimes in the ODT only represent the loss rate induced by collisions from atoms in the atomic beam and background gas and do not include any additional losses that might occur due to hetero-atomic light assisted collisions if the atomic clouds were well overlapped [35].

B. The Zeeman Slower

Of interest to the design of the Zeeman slower was the effect of slower length and the intensity of the slowing light on loading rate. For operation of the Rb Zeeman slower, an additional repump laser was needed to optically pump atoms out of the lower hyperfine ground state. This is not needed for Li as the larger magnetic field ensures the slowing transition is closed. For optimizing the MOT loading rate, the expected detuning and field profile was set based on the virtual slower simulations, then each coil was scanned about its set point to optimize the loading rate. In all cases, the optimal setpoint was within a few percent of the predicted value. This process was repeated for increasing η until a decrease in loading rate was observed. Table I shows the relevant operational parameters used for testing. We were able to observe small MOTs for both species when the slowing beam is off. Activating the slowing beam and using the magnetic field produced by the quadrupole coils of the MOT as the sole Zeeman slower leads to a factor of 6-8 improvement in loading rate for both species. Activating the remaining Zeeman slower field further improved the loading by a factor of 5 and 12 for Li and Rb, respectively.

TABLE I. Loading parameters for both MOTs.

	Rb	Li
Slowing Beam Detuning (MHz)	-85	-76
Slowing Beam Power (mW)	15	40
MOT Pump Beam Detuning (MHz) ^a	-15	-45
MOT Repump Beam Detuning (MHz) ^b	0	-40
MOT Pump Beam Power (mW) ^c	35	30
MOT Repump Beam Power (mW) ^c	10	40
MOT Axial Gradient (G/cm)	15.4	49

^a Detuning for ^{85}Rb is with respect to the $F = 3 \rightarrow F' = 4$ transition. Detuning for ^6Li is with respect to the $F = 3/2 \rightarrow F' = 5/2$ transition.

^b Detuning for ^{85}Rb is with respect to the $F = 2 \rightarrow F' = 3$ transition. Detuning for ^6Li is with respect to the $F = 1/2 \rightarrow F' = 5/2$ transition.

^c Beams have a radius of 9 mm, and the power is split between three retroflected arms of the MOT

To change the slower length, the number of coils activated was varied while monitoring the loading rate. To predict the loading rate, the flux of slowed atoms passing through the MOT was calculated by integrating over the angular and velocity distribution of atoms leaving the effusive source. For each velocity, there is a critical exit angle for atoms leaving the effusive source above which they will miss the MOT after slowing. This angle is determined from basic kinematics given the constant deceleration along the slower and does not account for the added reduction in captured atoms due to transverse heating. This angle, along with the capture velocity of the slower, sets the limits of integration which in turn determine the capturable flux. The scaling of loading rate with length is highly sensitive to the velocity group within the distribution being slowed. For Li, the velocity distribution

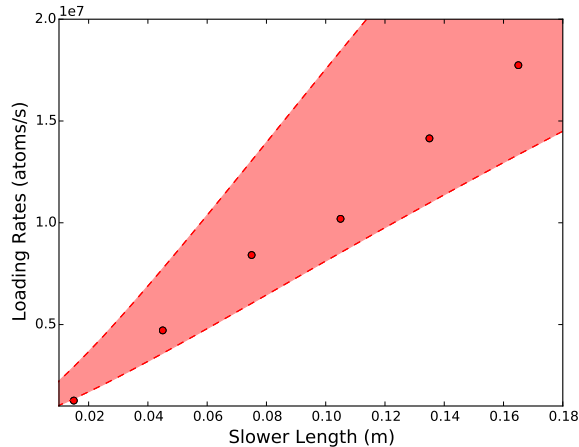


FIG. 7. The MOT loading rate for Li as function slower length at a source temperature of 630 K. The shaded region is the expected loading rate based on our model given a ± 5 K temperature uncertainty and 10% uncertainty in microtube number.

is peaked at 1700 m/s, while the maximum capture velocity is approximately 600 m/s. As a result, the atoms slowed are from the low velocity tail of the distribution. Directly integrating the Maxwell-Boltzmann distribution up to capture velocity for small velocities leads to v^4 scaling. Combining this with the \sqrt{L} scaling for the capture velocity, one may expect to see quadratic scaling of the loading rate with initial increases in slower length if the divergence of the atomic beam is disregarded. In contrast, for Rb the distribution is peaked at much lower velocity of 300 m/s and atoms are predominantly captured from the linear region of distribution resulting in linear scaling of capture velocity with slower length using the same argument. Experimentally, we observe linear scaling of the loading rate for both species, and not quadratic for Li, which is in good agreement with our numerical simulation. The reduced loading rate for Li is a result of the larger divergence of the atomic beam upon exiting the slower, as compared to Rb, given its much higher initial velocity and lighter mass.

It is challenging to accurately predict the loading rate for two reasons: 1) it is difficult to properly estimate the actual area of the effusive source outlet and account for microtube misalignment and the atomic emission from gaps and 2) it is difficult to know the exact source temperature to which the flux is exponentially sensitive. In Figures 7 and 8, we compare the measured and predicted loading rates on slower length, and we find that the model provides reasonable estimates for the expected flux given our uncertainty in the source temperature and a microtube array assembly (10% uncertainty in microtube number).

Finally the effect of the slowing beam intensity on loading rate was investigated. For Li, we observed an improved loading rate with beam power while for Rb we

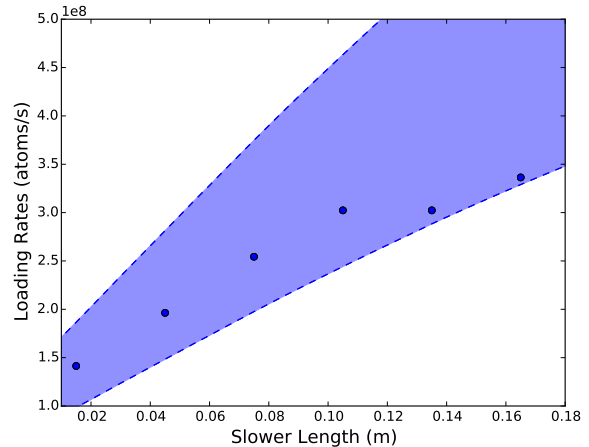


FIG. 8. The MOT loading rate for Rb as function slower length at a source temperature of 370 K. The shaded region is the expected loading rate based on our model given a ± 3 K temperature uncertainty and 10% uncertainty in microtube number.

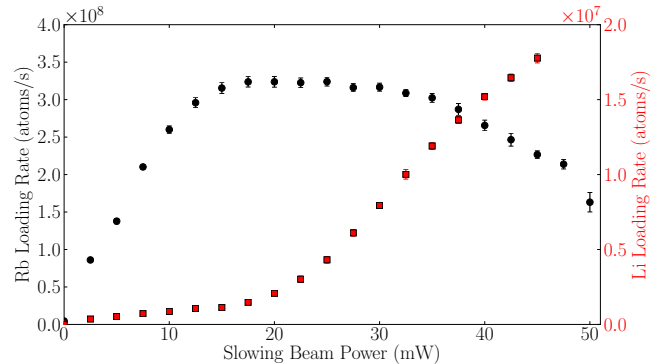


FIG. 9. The effect of slowing beam power on the MOT loading rate for Li (red squares) and Rb (black dots). We attribute the roll over of the Rb loading rate as resulting from atoms being stopped prior to reaching the MOT at the higher slower intensities.

saw decrease in loading rate at higher intensities. We attribute the roll over of the Rb loading rate as resulting from atoms being stopped prior to reaching the MOT at the higher slower intensities. The Rb beam is more susceptible to this than the Li beam because of its much lower exit velocity and smaller slowing field.

III. CONCLUSION

We have demonstrated a simple multi-species effusive source and slower design which is applicable to a range of different atomic physics applications. The short slower length was chosen due to the linear scaling of loading rate with slower length for both species. For Li, the linear

scaling was a result of divergence of the atomic beam, while for Rb it was due to the peaking of the thermal distribution of velocities leaving the source. These effects are not unique to species studied here, but universal to the design of a Zeeman slower for any atomic species. In addition, the design of our slower is made more compact by utilizing the quadruple magnetic field for the MOT as a secondary slowing field. We achieve a maximum loading rate of 3.5×10^8 atoms/s for Rb and 2×10^7 atoms/s for Li which is consistent with the expected performance of the slower at the operational temperatures of the effusive sources. The design of the effusive source and the slower makes the apparatus easily modified to facilitate

the cooling of other atomic species.

IV. ACKNOWLEDGMENTS

The authors also acknowledge financial support from the Canadian Institute for Advanced Research (CIFAR), the Natural Sciences and Engineering Research Council of Canada (NSERC / CRSNG), and the Canadian Foundation for Innovation (CFI). This work was done under the auspices of the Center for Research on Ultra-Cold Systems (CRUCS). The authors would also like to thank Florian Schreck for the microtubes used for both sources.

-
- [1] M. Taglieber, A. Voigt, T. Aoki, T. W. Hänsch, and K. Dieckmann, *Phys. Rev. Lett.* **100**, 010401 (2008).
- [2] A. Trenkwalder, C. Kohstall, M. Zaccanti, D. Naik, A. I. Sidorov, F. Schreck, and R. Grimm, *Phys. Rev. Lett.* **106**, 115304 (2011).
- [3] G. Roati, F. Riboli, G. Modugno, and M. Inguscio, *Phys. Rev. Lett.* **89**, 150403 (2002).
- [4] S. Ospelkaus, C. Ospelkaus, L. Humbert, K. Sengstock, and K. Bongs, *Phys. Rev. Lett.* **97**, 120403 (2006).
- [5] I. Titvinidze, M. Snoek, and W. Hofstetter, *Phys. Rev. Lett.* **100**, 100401 (2008).
- [6] S.-K. Tung, C. Parker, J. Johansen, C. Chin, Y. Wang, and P. S. Julienne, *Phys. Rev. A* **87**, 010702 (2013).
- [7] G. Modugno, M. Modugno, F. Riboli, G. Roati, and M. Inguscio, *Phys. Rev. Lett.* **89**, 190404 (2002).
- [8] G. Thalhammer, G. Barontini, L. De Sarlo, J. Catani, F. Minardi, and M. Inguscio, *Phys. Rev. Lett.* **100**, 210402 (2008).
- [9] M. Guglielmino, V. Penna, and B. Capogrosso-Sansone, *Phys. Rev. A* **82**, 021601 (2010).
- [10] M. Jag, M. Zaccanti, M. Cetina, R. S. Lous, F. Schreck, R. Grimm, D. S. Petrov, and J. Levinsen, *Phys. Rev. Lett.* **112**, 075302 (2014).
- [11] R. Pires, J. Ulmanis, S. Häfner, M. Repp, A. Arias, E. D. Kuhnle, and M. Weidemüller, *Phys. Rev. Lett.* **112**, 250404 (2014).
- [12] K. K. Ni, S. Ospelkaus, M. H. G. de Miranda, A. Pe'er, B. Neyenhuis, J. J. Zirbel, S. Kotochigova, P. S. Julienne, D. S. Jin, and J. Ye, *Science* **322**, 231 (2008).
- [13] F. M. Spiegelhalter, A. Trenkwalder, D. Naik, G. Kerner, E. Wille, G. Hendl, F. Schreck, and R. Grimm, *Phys. Rev. A* **81**, 043637 (2010).
- [14] J. W. Park, S. A. Will, and M. W. Zwierlein, *Phys. Rev. Lett.* **114**, 205302 (2015).
- [15] D. DeMille, *Phys. Rev. Lett.* **88**, 067901 (2002).
- [16] A. Micheli, G. K. Brennen, and P. Zoller, *Nature Physics* **2**, 341 (2006).
- [17] K. R. A. Hazzard, B. Gadway, M. Foss-Feig, B. Yan, S. A. Moses, J. P. Covey, N. Y. Yao, M. D. Lukin, J. Ye, D. S. Jin, and A. M. Rey, *Phys. Rev. Lett.* **113**, 195302 (2014).
- [18] M. Aymar and O. Dulieu, *The Journal of Chemical Physics* **122**, 204302 (2005), <http://dx.doi.org/10.1063/1.1903944>.
- [19] G. Modugno, G. Ferrari, G. Roati, R. J. Brecha, A. Simoni, and M. Inguscio, *Science* **294**, 1320 (2001), <http://www.sciencemag.org/content/294/5545/1320.full.pdf>.
- [20] V. V. Ivanov, A. Khramov, A. H. Hansen, W. H. Dowd, F. Münchow, A. O. Jamison, and S. Gupta, *Phys. Rev. Lett.* **106**, 153201 (2011).
- [21] F. Schreck, G. Ferrari, K. L. Corwin, J. Cubizolles, L. Khaykovich, M. Mewes, and C. Salomon, *Phys. Rev. A* **64**, 011402 (2001).
- [22] Z. Hadzibabic, C. A. Stan, K. Dieckmann, S. Gupta, M. W. Zwierlein, A. Görlitz, and W. Ketterle, *Phys. Rev. Lett.* **88**, 160401 (2002).
- [23] J. Catani, G. Barontini, G. Lamporesi, F. Rabatti, G. Thalhammer, F. Minardi, S. Stringari, and M. Inguscio, *Phys. Rev. Lett.* **103**, 140401 (2009).
- [24] S. Nascimbene, N. Navon, K. Jiang, F. Chevy, and C. Salomon, *Nature* **463**, 1057 (2010).
- [25] M. R. Walkiewicz, P. J. Fox, and R. E. Scholten, *Review of Scientific Instruments* **71**, 3342 (2000).
- [26] P. Clausing, *Journal of Vacuum Science and Technology* **8**, 636 (1971).
- [27] H. C. W. Beijerinck and N. F. Verster, *Journal of Applied Physics* **46**, 2083 (1975).
- [28] C. A. Stan and W. Ketterle, *Review of Scientific Instruments* **76**, 063113 (2005).
- [29] E. Wille, F. Spiegelhalter, G. Kerner, D. Naik, A. Trenkwalder, G. Hendl, F. Schreck, R. Grimm, T. Tiecke, J. Walraven, S. Kokkelmans, E. Tiesinga, and P. Julienne, *Phys. Rev. Lett.* **100**, 053201 (2008).
- [30] R. Senaratne, S. V. Rajagopal, Z. A. Geiger, K. M. Fujiwaram, V. Lebedev, and D. M. Weld, "Effusive atomic oven nozzle design using a microcapillary array," (2014), [arXiv:1407.6391](https://arxiv.org/abs/1407.6391).
- [31] S. C. Bell, M. Junker, M. Jasperse, L. D. Turner, Y.-J. Lin, I. B. Spielman, and R. E. Scholten, *Review of Scientific Instruments* **81**, 013105 (2010).
- [32] K. Dieckmann, R. J. C. Spreeuw, M. Weidemüller, and J. T. M. Walraven, *Phys. Rev. A* **58**, 3891 (1998).
- [33] T. G. Tiecke, S. D. Gensemer, A. Ludewig, and J. T. M. Walraven, *Phys. Rev. A* **80**, 013409 (2009).
- [34] S. Dutta, J. Lorenz, A. Altaf, D. S. Elliott, and Y. P. Chen, *Phys. Rev. A* **89**, 020702 (2014).
- [35] K. Ladouceur, B. G. Klappauf, J. V. Dongen, N. Rauhut, B. Schuster, A. K. Mills, D. J. Jones, and K. W. Madison, *J. Opt. Soc. Am. B* **26**, 210 (2009).

- [36] S. Ospelkaus, C. Ospelkaus, R. Dinter, J. Fuchs, M. Nakat, K. Sengstock, and K. Bongs, *Journal of Modern Optics* **54**, 661 (2007), <http://dx.doi.org/10.1080/09500340600777763>.
- [37] A. Ridinger, S. Chaudhuri, T. Salez, U. Eismann, D. Fernandes, K. Magalhes, D. Wilkowski, C. Salomon, and F. Chevy, *The European Physical Journal D* **65**, 223 (2011).
- [38] J. Goldwin, S. Inouye, M. L. Olsen, B. Newman, B. D. DePaola, and D. S. Jin, *Phys. Rev. A* **70**, 021601 (2004).
- [39] M. Taglieber, A.-C. Voigt, F. Henkel, S. Fray, T. W. Hänsch, and K. Dieckmann, *Phys. Rev. A* **73**, 011402 (2006).
- [40] W. Gunton, M. Semczuk, and K. W. Madison, *Phys. Rev. A* **88**, 023624 (2013).
- [41] C. J. Dedman, J. Nes, T. M. Hanna, R. G. Dall, K. G. H. Baldwin, and A. G. Truscott, *Review of Scientific Instruments* **75** (2004).
- [42] R. Napolitano, S. Zilio, and V. Bagnato, *Optics Communications* **80**, 110 (1990).
- [43] I. R. Hill, Y. B. Ovchinnikov, E. M. Bridge, E. A. Curtis, and P. Gill, *Journal of Physics B: Atomic, Molecular and Optical Physics* **47**, 075006 (2014).
- [44] G. E. Marti, R. Olf, E. Vogt, A. Öttl, and D. M. Stamper-Kurn, *Phys. Rev. A* **81**, 043424 (2010).
- [45] A. Mosk, S. Kraft, M. Mudrich, K. Singer, W. Wohlleben, R. Grimm, and M. Weidemüller, *Applied Physics B* **73**, 791 (2001).
- [46] B. Deh, W. Gunton, B. G. Klappauf, Z. Li, M. Semczuk, J. Van Dongen, and K. W. Madison, *Phys. Rev. A* **82**, 020701 (2010).
- [47] A. Paris-Mandoki, M. D. Jones, J. Nute, J. Wu, S. Warriar, and L. Hackermüller, *Review of Scientific Instruments* **85**, 113103 (2014).
- [48] E. E. Edwards, *Construction of Apparatus and First Experiments Investigating Dynamics of Bose-Einstein Condensate in Disordered Optical Lattices*, Ph.D. thesis, University of Maryland, College Park, College Park, MD 20742, United States (2009).
- [49] B. P. Anderson and M. A. Kasevich, *Phys. Rev. A* **63**, 023404 (2001).
- [50] W. J. Bowden, *An Experimental Apparatus for the Laser Cooling of Lithium and Rubidium*, Master's thesis, University of British Columbia.
- [51] D. R. Olander, R. H. Jones, and W. J. Siekhaus, *Journal of Applied Physics* **41**, 4388 (1970).
- [52] G. R. Hanes, *Journal of Applied Physics* **31**, 2171 (1960).
- [53] N. Ramsey, *Molecular beams*, International series of monographs on physics (Clarendon Press, 1963).
- [54] J. Van Dongen, C. Zhu, D. Clement, G. Dufour, J. L. Booth, and K. W. Madison, *Phys. Rev. A* **84**, 022708 (2011).
- [55] J. Van Dongen, C. Zhu, D. Clement, G. Dufour, J. L. Booth, and K. W. Madison, *Phys. Rev. A* **84**, 022708 (2011).

MOT magneto-optical trap

ODT optical dipole trap